Desalination and Water Treatment
www.deswater.com
doi: 10.5004/dwt.2020.25863

194 (2020) 69–84
August

Simultaneous nitritation, anammox, and denitrification (SNAD) process in a membrane bioreactor: start-up, optimization, and membrane fouling behavior

Zhaozhao Wang[a,b], Peng Gao[a,b], Lina Yan[c], Dan Zhao[a,b], Ying Ji[a,b], Huan Zhang[a,b], Simin Li[a,b,*]

[a]*College of Energy and Environmental Engineering, Hebei University of Engineering, Handan 056038, China, Tel. +8617831917609; emails: 18303233729@163.com (S. Li), W-Z-Z@163.com (Z. Wang), 13082137058@163.com (P. Gao), 18732059211@163.com (D. Zhao), 18244606382@139.com (Y. Ji), zh982479127@163.com (H. Zhang)*
[b]*Center for Water Pollution Control and Water Ecological Remediation, Hebei University of Engineering, Handan 056038, China*
[c]*College of Environmental and Energy Engineering, Beijing University of Technology, Beijing 100124, China, email: yanlina01@126.com (L. Yan)*

Received 15 November 2019; Accepted 17 March 2020

ABSTRACT

An experiment was conducted in a membrane bioreactor (MBR) to investigate the start-up, optimization, and membrane fouling behavior of a simultaneous nitritation, anammox, and denitrification (SNAD) process for the treatment of nitrogen-containing organic wastewater. The start-up process of SNAD included three periods: first, anammox flocs were incubated in the bioreactor and enriched using a short hydraulic retention time (HRT) from 24 h to 4.0 h, this treatment enhanced the anammox start-up process, and a nitrogen removal efficiency (NRE) of 82.5% and nitrogen removal rate (NRR) of 0.49 kg/(m^3 d) were achieved. Second, a completely autotrophic nitrogen removal over nitrite (CANON) process that incorporated aerobic ammonium oxidizing bacteria (AerAOB) and anaerobic ammonium-oxidizing bacteria (AnAOB) was started up through the optimization of intermittent aeration (non-aeration time to aeration time of 4.0:10 min), in this process, the dissolved oxygen (DO) remained in the range of 0.6–0.8 mg/L. Third, the SNAD process was started up by introducing organic carbon (sodium acetate), ammonium removal efficiency (ARE) of 91.2%, NRE of 77.9%, and chemical oxygen demand (COD) removal efficiency (CRE) of 82.4% were achieved at a C/N ratio of 0.5. The SNAD process was further optimized by regulating the C/N ratio. The optimum synergy of the AnAOB, AnAOB, and denitrifying bacteria (DNB) was achieved at a C/N ratio of 1.0, and the ARE, NRE, and CRE were 91.7%, 86.4%, and 85%, respectively. A SNAD mass balance model was established and indicated that the anammox process played a dominant role in nitrogen removal, the contribution of the anammox pathway to nitrogen removal was 64.7%. The membrane fouling rate was reduced due to an increase in the particle size resulting from the increase in the extracellular polymeric substances (EPS) content and the ratio of the protein to carbohydrate concentrations in the EPS (EPS_p/EPS_c). Fourier transform infrared spectroscopy (FT-IR) analysis showed that protein and carbohydrates were the main components of the membrane foulants. Moreover, the composition of the membrane foulants exhibited little change during the operation.

Keywords: Nitritation; Anammox; Denitrification; C/N ratio; Membrane fouling

* Corresponding authors.

1. Introduction

The eutrophication of slow-flowing water bodies resulting from nitrogen leaching has become a significant concern and has attracted worldwide attention. The economical and efficient removal of nitrogen from wastewater is currently a trending research topic in the wastewater treatment field. The traditional biological nitrogen removal process relies first on aerobic ammonium-oxidizing bacteria (AerAOB) and nitrite-oxidizing bacteria (NOB) to complete the nitrification process, subsequently, in the denitrification process, denitrifying bacteria (DNB) convert nitrate to dinitrogen to remove nitrogen from sewage/wastewater [1,2]. Since the denitrification process requires a carbon source as an electron donor, the traditional biological nitrogen removal process is significantly limited when the wastewater has a low C/N ratio [3,4].

Anaerobic ammonium oxidation (anammox) technology is currently the most economical autotrophic nitrogen removal technology, in this process, ammonium is oxidized by anaerobic ammonium-oxidizing bacteria (AnAOB) using nitrite as an electron donor to convert ammonium into dinitrogen under anaerobic or anoxic conditions. The reaction is defined in Eq. (1):

$$NH_4^+ + 1.32NO_2^- + 0.066HCO_3^- + 0.13H^+ \rightarrow 1.02N_2 + 0.26NO_3^- + 0.066CH_2O_{0.5}N_{0.15} + 2.03H_2O \quad (1)$$

At present, autotrophic nitrogen removal processes based on anammox include two types: single reactor for high ammonia removal over nitrite-anaerobic ammonium oxidation (SHARON–ANAMMOX) and completely autotrophic nitrogen removal over nitrite (CANON). Compared to the traditional biological nitrogen removal process, the autotrophic nitrogen removal process has the advantages of low energy consumption, no additional carbon source, and low sludge production [5–7]. The coupling of nitritation and anammox is achieved in the one-stage CANON process by controlling the dissolved oxygen (DO) content, as shown in Eq. (2), the CANON process has economic advantages over the two-stage SHARON–ANAMMOX process [8,9].

$$NH_4^+ + 0.85O_2 \rightarrow 0.44N_2 + 0.11NO_3^- + 0.14H^+ + 1.43H_2O \quad (2)$$

AnAOB are autotrophic bacteria living in anaerobic conditions, they have a slow growth rate, and long generation time [10]. Some researchers have attempted to use the membrane bioreactor (MBR) process to achieve complete retention of AnAOB, this resulted in high activities of the culture [11]. Wang et al. [12] successfully started up an anammox process in an MBR reactor, the process operated for 49 d with the maximum and achieved a nitrogen removal rate (NRR) of 0.345 kg/(m^3 d). Hendrickx et al. [13] achieved enrichment of AnAOB (mainly *Candidatus Brocadia fulgida*) even at a low temperature (10°C) in an MBR [13].

Only approximately 90% of the total nitrogen (TN) in the form of ammonia and nitrite can be removed by AnAOB, and about 10% of the TN remains in the effluent. Since most wastewater contains both organic matter and nitrogen, AnAOB are inhibited to various degrees, depending on the concentration of organic matter [14]. In recent years, it has been discovered that AnAOB and DNB can coexist in the same reactor and they exhibit synergism, which provides a new pathway for simultaneous nitrogen and carbon removal in the treatment of nitrogen-containing organic wastewater [15]. Simultaneous nitritation, anammox, and denitrification (SNAD) in a single-stage reactor has become an efficient approach to improve the nitrogen removal performance in wastewater treatment [16]. MBR reactors have been utilized to achieve rapid startup and operational stability of the SNAD process. Wang et al. [17] used an intermittent aeration MBR to treat synthetic wastewater and achieved SNAD after 197 d of operation. Zhao et al. [18] successfully achieved SNAD in an oxygen-limited MBR reactor, and high carbon and NRRs were observed at a C/N ratio of 0.52, the nitrogen removal efficiency (NRE) was 94.86%, and the chemical oxygen demand (COD) removal efficiency (CRE) was 98.91% [18]. Few studies have investigated strategies to optimize the SNAD process. Furthermore, the characteristics of the membrane fouling behavior in the MBR-SNAD process require an in-depth analysis to gain insights into the sustainable operation and the underlying mechanisms of the system.

The objectives of this study are (1) to initiate the SNAD process in an MBR, (2) to optimize the SNAD process by regulating the C/N ratio, (3) to investigate the membrane fouling behavior to provide technical support for the startup, and operation of the SNAD process for the treatment of nitrogen-containing organic wastewater.

2. Materials and methods

2.1. Experimental setup and operational conditions

The schematic diagram of the bench-scale SNAD-MBR plant is depicted in Fig. 1. The reactor and the water tanks were made of plexiglass, and the effective volume of the reactor was 53.50 L. The plant included a programmable logic controller (PLC) and a data acquisition system that controlled the flows. The hollow fiber membrane module (pore size, 0.03 μm, surface area, 0.52 m^2, made of polyvinylidene fluoride, obtained from Hangzhou Mina Membrane Technology Corporation, China) was operated at a constant flux (13.0 L/(m^2 h)) with intermittent suction (9.0-min suction and 1.0 min rest). The transmembrane pressure (TMP) was monitored by a pressure gauge, when the pressure reached 0.5 bar, off-line membrane cleaning was initiated using 0.5% NaClO. The reactor had a mixer to keep the sludge in suspension. A microporous aeration disc was installed at the bottom of the reactor and was connected to an air compressor to supply the DO to the reactor. A pH-DO sensor (Multi 340i, WTW Corporation, Germany) was used to monitor the DO and pH levels in the aerobic membrane tank. A circulating water bath system was used to maintain the temperature at 30°C ± 2.0°C. The MBR plant was operated without sludge discharge during the entire period of 462 d.

The experimental process was divided into four periods and 19 phases. The first period was the anammox startup period (phase I–V). The second period was the CANON startup period, which included eight phases, the sequencing

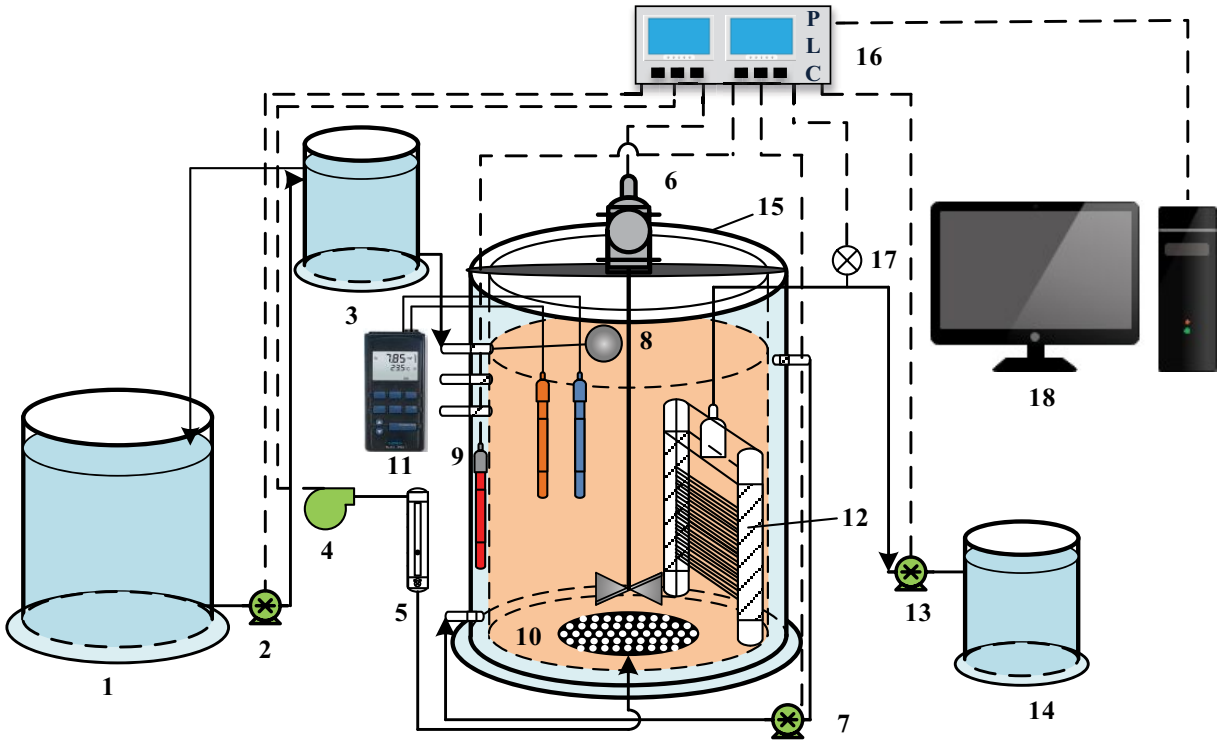

Fig. 1. Schematic diagram of the bench-scale SNAD-MBR plant. (1) influent tank, (2) influent pump, (3) high-level water tank, (4) air compressor, (5) flowmeter, (6) mixer, (7) water bath circulating pump, (8) floating ball valve, (9) heating rod, (10) aeration disc, (11) DO/pH sensor, (12) hollow fiber membrane module, (13) permeate pump, (14) effluent tank, (15) reactor, (16) programmable logic controller (PLC), (17) pressure gauge, (18) computer.

batch operation occurred in phases VI–X and phases XI–XIII represented the continuous operation. The third period was the SNAD startup period (phase XIV), in which organic carbon (sodium acetate) was introduced into the system. The fourth period was the SNAD optimization period (phase XV–XIX), in which the influent C/N ratio was regulated. The operational conditions of the experimental process are listed in Table 1.

2.2. Characteristics of the feed wastewater and seed sludge

The seed sludge (flocculent anammox sludge) was obtained from a pilot-scale anammox-upflow anaerobic sludge bed (UASB) reactor used for the treatment of high-nitrogen wastewater, the reactor had been operated stably for two years. The initial concentration of the mixed liquor suspended solids (MLSS) in the reactor was approximately 2,000 mg/L. In addition, activated sludge samples obtained from the east wastewater treatment plant of Handan, which employs a *T*-type oxidized ditch process, were inoculated into the reactor to enrich AerAOB after the anammox startup period. Subsequently, the MLSS concentration in the reactor increased to about 2,500 mg/L. The synthetic sewage was composed of NH_4Cl, $NaNO_2$, NH_4Cl, NaAc, $NaHCO_3$, KH_2PO_4, $MgSO_4{\cdot}7H_2O$, $CaCl_2{\cdot}2H_2O$, and $FeSO_4$. The trace element solution I consisted of $KHCO_3$ (1,250 mg/L), KH_2PO_4 (25 mg/L), $CaCl_2{\cdot}2H_2O$ (300 mg/L), $MgSO_4{\cdot}7H_2O$ (200 mg/L), and $FeSO_4$ (6.25 mg/L), the trace element solution II consisted of EDTA (15,000 mg/L), $ZnSO_4{\cdot}7H_2O$ (430 mg/L), $CoCl_2{\cdot}6H_2O$ (240 mg/L), $MnCl_2{\cdot}4H_2O$ (990 mg/L), $CuSO_4{\cdot}5H_2O$ (250 mg/L), $NaMoO_4{\cdot}2H_2O$ (220 mg/L), $NiCl_2{\cdot}6H_2O$ (190 mg/L), $NaSeO_4{\cdot}10H_2O$ (210 mg/L), H_3BO_4 (14 mg/L), and $NaWO_4{\cdot}2H_2O$ (50 mg/L). The dosage of the trace element solutions I and II was 1.0 ml/L. The C/N ratio was defined as the COD/TN ratio in the influent, the concentrations of nitrogen and organic matter during the operation are listed in Table 1.

2.3. Analytical methods

2.3.1. Wastewater and sludge analyses

The concentrations of COD, NH_4^+–N, NO_3^-–N, NO_2^-–N, TN, MLSS, mixed liquor volatile suspended solids (MLVSS), and the sludge volume index (SVI) were determined using standard methods [19]. The particle size of the flocculent sludge was measured using a laser particle size analyzer (Mastersizer 2000, Malvern, UK). The particle size of the granular sludge was determined using a standard wet screening method [20].

The ammonium removal efficiency (ARE), NRE, the nitrogen loading rate (NLR), NRR, CRE, ΔNO_2^-–N/ΔNH_4^+–N ratio, ΔNO_3^-–N/ΔNH_4^+–N ratio, and ΔNO_3^-–N/ΔTN ratio were calculated with the following equations:

$$\mathrm{ARE} = \frac{NH_4^+ - N_{Inf} - NH_4^+ - N_{Eff}}{NH_4^+ - N_{Inf}} \times 100\% \quad (3)$$

Table 1
Operational conditions and substrates of the startup and optimization periods of the SNAD process

Operation strategy	Phases	HRT (h)	Periods (d)	C/N ratio	COD (mg/L)	NH_4^+–N (mg/L)	NO_2^-–N (mg/L)	$R_{s:a}$ (min:min)
Anammox startup	I	24	1–55			71.40	92.90	
	II	12	56–110			74.20	91.80	
	III	8.0	111–142			72.60	92.20	
	IV	6.0	143–166			72.10	91.50	
	V	4.0	167–188			71.50	91.40	
CANON startup	VI	12	190–206			201.02	102.93	4.0:10
	VII	12	208–220			197.14	61.41	2.0:10
	VIII	12	222–234			187.08	23.04	2.0:20
	IX	12	236–272			192.67	21.68	4.0:15
	X	12	274–296			200.32	21.61	4.0:10
	XI	4.0	300–308			200.08	21.78	4.0:10
	XII	6.0	310–326			201.08	22.21	4.0:10
	XIII	8.0	328–340			200.13	20.85	4.0:10
SNAD startup	XIV	8.0	342–380	0.5	101.6	187.5	19.8	4.0:15
	XV	8.0	381–391	0.25	51.8	199.9	23.6	4.0:8
SNAD optimization	XVI	8.0	392–412	1.0	198.4	194.4	19.8	4.0:10
	XVII	8.0	414–432	2.0	401.2	205.3	23.1	4.0:15
	XVIII	8.0	434–446	3.0	596.8	194.7	23.1	4.0:15
	XIX	8.0	448–462	1.0	197.8	194.4	19.8	4.0:10

$R_{s:a}$: the ratio of stop-aeration time to aeration time.

$$\mathrm{NRE} = \frac{\mathrm{TN_{Inf}} - \mathrm{TN_{Eff}}}{\mathrm{TN_{Inf}}} \times 100\% \quad (4)$$

$$\mathrm{NLR} = \frac{\mathrm{TN_{Inf}}}{\mathrm{HRT}} \quad (5)$$

$$\mathrm{NRR} = \frac{\mathrm{TN_{Inf}} - \mathrm{TN_{Eff}}}{\mathrm{HRT}} \quad (6)$$

$$\mathrm{CRE} = \frac{\mathrm{COD_{Inf}} - \mathrm{COD_{Eff}}}{\mathrm{COD_{Inf}}} \times 100\% \quad (7)$$

$$\frac{\Delta \mathrm{NO_2^-} - \mathrm{N}}{\Delta \mathrm{NH_4^+} - \mathrm{N}} = \frac{\mathrm{NO_2^-} - \mathrm{N_{Inf}} - \mathrm{NO_2^-} - \mathrm{N_{Eff}}}{\mathrm{NH_4^+} - \mathrm{N_{Inf}} - \mathrm{NH_4^+} - \mathrm{N_{Eff}}} \quad (8)$$

$$\frac{\Delta \mathrm{NO_3^-} - \mathrm{N}}{\Delta \mathrm{NH_4^+} - \mathrm{N}} = \frac{\mathrm{NO_3^-} - \mathrm{N_{Inf}} - \mathrm{NO_3^-} - \mathrm{N_{Eff}}}{\mathrm{NH_4^+} - \mathrm{N_{Inf}} - \mathrm{NH_4^+} - \mathrm{N_{Eff}}} \quad (9)$$

$$\frac{\Delta \mathrm{NO_3^-} - \mathrm{N}}{\Delta \mathrm{TN}} = \frac{\mathrm{NO_3^-} - \mathrm{N_{Inf}} - \mathrm{NO_3^-} - N_{\mathrm{Eff}}}{\mathrm{TN_{Inf}} - \mathrm{TN_{Eff}}} \quad (10)$$

where $\mathrm{NH_4^+}$–$\mathrm{N_{Inf}}$, $\mathrm{NO_2^-}$–$\mathrm{N_{Inf}}$, $\mathrm{NO_3^-}$–$\mathrm{N_{Inf}}$, $\mathrm{TN_{Inf}}$, and $\mathrm{COD_{In}}$ are the concentrations of $\mathrm{NH_4^+}$–N, $\mathrm{NO_2^-}$–N, $\mathrm{NO_3^-}$–N, TN, and COD (mg/L) in the influent, respectively, $\mathrm{NH_4^+}$–$\mathrm{N_{Eff}}$, $\mathrm{NO_2^-}$–$\mathrm{N_{Eff}}$, $\mathrm{NO_3^-}$–$\mathrm{N_{Eff}}$, $\mathrm{TN_{Eff}}$, and $\mathrm{COD_{Eff}}$ are the concentrations of $\mathrm{NH_4^+}$–N, $\mathrm{NO_2^-}$–N, $\mathrm{NO_3^-}$–N, TN, and COD (mg/L) in the effluent, respectively, HRT is the hydraulic retention time (d).

2.3.2. Analysis of the activities of the functional bacteria

The schematic diagram of the sequencing batch reactor (A, B, C, and D) is shown in Fig. 2. A 250 mL serum bottle was used in the sequencing batch tests. First, the sludge mixture was collected from the SNAD-MBR reactor and washed using deionized water to remove the residue (this was repeated 3 times). Second, the sludge and 250 mL of a prepared matrix were added, and the serum bottle was placed on a magnetic stirrer. Finally, the magnetic stirrer was started, 5.0 mL of the mixture was extracted with a 10 mL syringe for centrifugation at 1.0 h intervals, and the concentrations of $\mathrm{NH_4^+}$–N, $\mathrm{NO_2^-}$–N, $\mathrm{NO_3^-}$–N, COD, and MLSS were determined [21,22]. The substrates used to determine the activities of the functional bacteria are shown in Table 2. The devices A, B, C, and D were used to measure the specific degradation rates of $\mathrm{NH_4^+}$–N, TN, $\mathrm{NO_2^-}$–N, and $\mathrm{NO_3^-}$–N, respectively, to characterize the activity of the functional bacteria.

2.3.3. Evaluation of membrane fouling behavior

The TMP (bar) data were corrected using the standard temperature (T, 20°C), as defined in Eq. (11):

$$\mathrm{TMP} = \mathrm{TMP_\theta} e^{0.023(\theta - 20)} \quad (11)$$

The membrane permeability was determined with Eq. (12):

$$L = \frac{J \times e^{-0.029(T-20)}}{\mathrm{TMP}} \quad (12)$$

where L is the membrane permeability (L/(m² h bar)), and J is the membrane flux (L/(m² h)).

The membrane fouling rate was determined with Eq. (13):

$$P_{DR} = \frac{L_s - L_e}{t} \quad (13)$$

where P_{DR} is the membrane fouling rate (L/(m² h² bar)), t is the running time (h), L_s is the permeability at startup, and L_e is the permeability at the end of the operation.

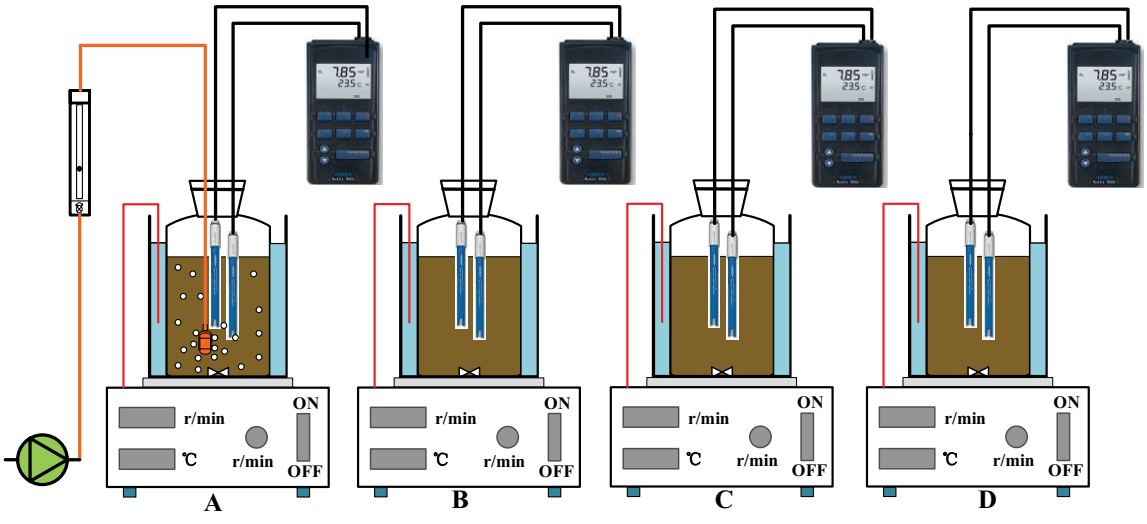

Fig. 2. Schematic diagram of the sequencing batch reactor.

Table 2
Substrates of the sequencing batch tests

Functional bacteria	AerAOB	AnAOB	$DNB_{NO_2^-N}$	$DNB_{NO_3^-N}$
(Testing reactor No.)	(A)	(B)	(C)	(D)
NH_4^+–N (mg/L)	90	90	0	0
NO_2^-–N (mg/L)	0	100	80	0
NO_3^-–N (mg/L)	0	0	0	60
COD (mg/L)	0	0	20–240	15–180

2.3.4. Sample extraction and fractionation

The concentration of extracellular polymeric substances (EPS) was determined using a heating method [23]. The sludge mixture collected from the SNAD-MBR reactor was centrifuged at 12,000× g for 15 min. Next, the soluble microbial products SMP were obtained by filtering the supernatant through a 0.45 μm membrane filter. The sludge pellets were then re-suspended in the same amount of buffer solution, which consisted of 2.0 mM Na_3PO_4, 4.0 mM Na_2HPO_4, 9.0 mM NaCl, and 1.0 mM KCl. Subsequently, the mixture was heated for 2.0 h at 105°C in an oven and was then centrifuged at 12,000 × g for 15 min. The supernatant was microfiltered through a membrane with a pore size of 0.45 μm. The filtered sample represented the total amount of EPS. The EPS and SMP were normalized as the sum of carbohydrates and proteins, whose concentrations were determined using the modified Bradford method with bovine serum albumin as the standard and the anthrone–sulfuric acid colorimetric method with glucose as the standard, respectively [24].

2.3.5. Extraction of membrane foulants and Fourier transform infrared analysis

The fouled membrane module was removed from the SNAD-MBR reactor and flushed with pure water at the end of each cycle. Approximately 300 mL of washed liquid was placed in a dryer at 105°C for 24 h to obtain the dry foulants. Fourier transform infrared spectroscopy (FT-IR) (IRAffinity-1, Japan) was used to characterize the major functional groups of the organic matter in the membrane foulants. KBr pellets containing 0.5% (dry powder) of the sample were prepared and examined using the FT-IR spectrophotometer. The data were processed with OriginPro 8.0 software.

3. Results and discussion

3.1. Start-up of SNAD process

3.1.1. Start-up of the anammox process

The performance during the anammox start-up period (phase I–V) is shown in Fig. 3. At the beginning of phase I, the ARE, NRE, and NRR were only 28.1%, 22.4%, and 0.019 kg/(m^3 d), respectively, indicating low activity of the AnAOB during the adaption phase. After 15 d domestication, the AnAOB activity had increased significantly, and the ARE and NRE were 89.7% and 71.8%, respectively. The AnAOB activity was further enhanced by reducing the HRT (from 12 to 4.0 h) to increase the NLR in phase II–V. The ARE, NRE, and NRR reached 95%, 82.5%, and 0.49 kg/(m^3 d), respectively, in phase V, indicating an increase in AnAOB activity during the enrichment period.

The theoretical stoichiometry ratios of ΔNO_2^-–N/ΔNH_4^+–N and ΔNO_3^-–N/ΔNH_4^+–N (Eq. (1)) were 1.32 and 0.26, respectively, these values provide an indication of the anammox biochemical reactions in the reactors. The changes in the ratios of ΔNO_2^-–N/ΔNH_4^+–N and ΔNO_3^-–N/ΔNH_4^+–N during phase I–V are illustrated in Fig. 3. During the first 15 d, the AnAOB were in the adaptation phase, and the stoichiometry ratios differed from the theoretical values. Moreover, the AerAOB induced the conversion of NH_4^+–N into NO_2^-–N at high DO concentrations (8.0 mg/L) in the influent, which resulted in a higher ΔNO_3^-–N/ΔNH_4^+–N ratio than the theoretical ratio. Subsequently, the stoichiometry ratios fluctuated around the theoretical values, which indicated that the anammox reaction was occurring.

3.1.2. Start-up of the CANON process

The process performance during the CANON start-up period (phase VI–XIII) is shown in Fig. 3. The sequencing batch operation and intermittent aeration were conducive to the enrichment of AerAOB in the CANON process startup from phase VI to phase X. The concentrations of NH_4^+–N and NO_2^-–N increased to 201.02 mg/L and 102.93 mg/L, respectively. A sharp decrease was observed in the ARE and NRE to 50.5% and 56.8%, respectively, in phase VI and resulted from the inhibition of the AnAOB activity. This result was attributed to the lack of adaptation of the AnAOB due to the sudden increase in the DO concentration (0.2–0.4 mg/L). In phase VII, the concentration of NO_2^-–N in the influent was reduced to about 60 mg/L, and the $R_{s:a}$ was maintained at 2.0:10 to ensure that the DO concentration was in the range of 0.6–0.8 mg/L. The ARE showed a slight decrease, whereas the removal efficiency of NO_2^-–N was maintained above 90%. This was likely the result of the oxidation of NO_2^-–N by nitrite-oxidizing bacteria (NOB). The concentration of NO_2^-–N in the influent was reduced to about 23 mg/L to enrich the AerAOB, and the DO was maintained at 1.0–1.2 mg/L. In phase VIII, the influent concentration of NO_2^-–N was reduced to about 23 mg/L to acclimate the AOB, and the DO concentration was maintained at 1.0–1.2 mg/L. After 12 d of operation, the removal efficiencies of NO_2^-–N remained above 95%, but the ARE and NRE decreased to about 20% and 25%, respectively. These results indicate that the ARE did not increase with an

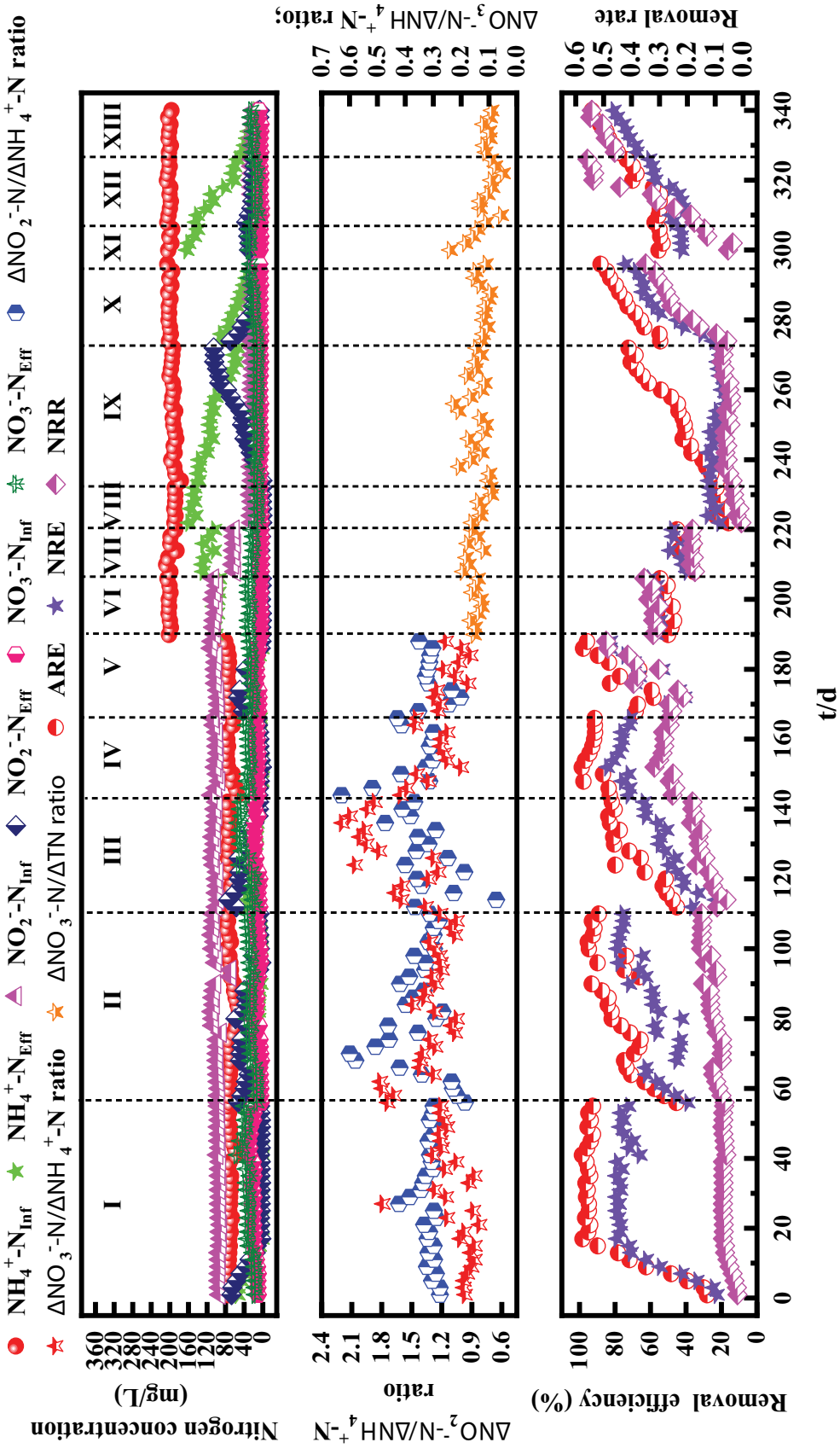

Fig. 3. Performance of the reactor during the different operational phases of the anammox and CANON start-up periods.

increase in the DO concentration. Conversely, the decrease in the ARE and NRE were partially attributed to the inhibition of the AnAOB activity resulting from the substrate (nitrite) reductions in the influent. Therefore, in phase IX, the $R_{s:a}$ was changed to 4.0:15 to obtain a DO concentration in the range of 0.6–0.8 mg/L. It was observed that the ARE increased to 72.31% as NO_2^-–N accumulated in the effluent as a result of the enrichment of AerAOB. Regardless, the NRE was maintained at about 15% due to the dormant period of the AnAOB. In phase X, the DO concentration decreased to 0.2–0.4 mg/L as the $R_{s:a}$ increased to 4:10. The AnAOB activity recovered and the AnAOB and AerAOB coexisted. The ARE and NRE were 74.4% and 60.9%, respectively, which suggested the successful startup of the CANON process. It should be noted that in the AerAOB enrichment period, the AnAOB activity was affected to some degree by the changes in the DO and feeding substrates. However, in general, the AnAOB activity was almost completely restored after the short-term inhibitions [25,26]. Due to the enrichment of AerAOB, the consumption of the low-concentration DO and the production of the nitrite accelerated the recovery of the AnAOB activity and thus enhanced the synergism of the two functional bacteria.

The continuous-flow operation was shifted from the sequencing batch operation to enhance the process performance in phase XI–XIII. The HRT was optimized to maintain a stable operation. The ARE, NRE, and NRR rapidly decreased to 19.6%, 3.8%, and 0.05 kg/(m^3 d) in phase XI from 88.1%, 74.7%, and 0.35 kg/(m^3 d), respectively in phase X as a result of the HRT reduction from 12 to 4.0 h. Subsequently, the HRT was increased to 8.0 h in phase XIII. After 12 d of operation, the ARE, NRE, and NRR recovered to 93.1%, 80.5%, and 0.54 kg/(m^3 d), respectively. Vázquez-Padín et al. [27] also successfully started up a granule-based CANON process and achieved ARE of 87.5%, NRE of 85%, and NRR of 0.45 kg/(m^3 d) during stable operation. In this study, the ΔNO_3^-–N/ΔTN ratio fluctuated around 0.125, which was in agreement with the theoretical stoichiometry ratio in the CANON process, this finding demonstrates the successful startup of the CANON process in phase XIII.

3.1.3. Start-up of the SNAD process

The process performance during the SNAD start-up period (phase XIV) is shown in Fig. 4. Short-chain organic carbon (sodium acetate) was introduced into the system in phase XIV. The NH_4^+–N concentration in the effluent increased significantly to 98.7 mg/L from 13.6 mg/L in phase XIII. The ARE, NRE, and NRR decreased to 50.9%, 41.4%, and 0.28 kg/(m^3 d) from 93.7%, 80.5%, and 0.54 kg/(m^3 d), respectively, in phase XIII. In addition, a substantial amount of COD was removed (50.9 mg/L) during the initial period, this was attributed to a decrease in the AerAOB activity as a result of the O_2 competition with heterotrophic bacteria. The DO concentration then increased from 0.2–0.4 mg/L to 0.6–0.8 mg/L due to a decrease in the $R_{s:a}$ value. After 38 d of operation, the AerAOB activity finally recovered and the activities of AnAOB and DNB were enhanced. The ARE, CRE, NRE, and NRR ultimately reached 91.2%, 77.9%, 82.4%, and 0.50 kg/(m^3 d), respectively. The activities of the functional bacteria were assessed after the successful startup of the SNAD process (Fig. 4b). The specific degradation rates of NH_4^+–N, TN, NO_2^-–N, and NO_3^-–N were 0.124, 0.180, 0.094, and 0.056 mgN/(mg MLSS d), respectively, indicating good activities of the AerAOB, AnAOB, and DNB, these results demonstrate the good synergistic effect of the different bacteria during nitrogen removal.

3.2. Optimization of the SNAD process

The optimization of the SNAD process was investigated by regulating the influent C/N ratios after the successful startup at a C/N ratio of 0.5. The process performance and the activities of the functional bacteria during the SNAD optimization period (phase XV–XIX) are presented in Fig. 5 and Table 3, respectively.

The results show that the average concentrations of NH_4^+–N, NO_2^-–N, and NO_3^-–N were 21.3, 9.3, and 21.3 mg/L at a C/N ratio of 0.25 in phase XV. ARE of 89.5%, NRE of 77.5%, and NRR of 0.54 kg/(m^3d) were achieved, these values were similar to those at a C/N ratio of 0.5 in phase XIV. The specific degradation rates of NH_4^+–N and TN were 0.126 and 0.182 mgN/(mg MLSS d), respectively, revealing slightly higher activities of the AerAOB and AnAOB in this phase than in phase XIV. After 12 d of operation, the C/N ratio was increased to 1.0 in phase XVI. The NH_4^+–N concentration in the effluent increased to 67.5 mg/L, resulting in a sharp decrease in the ARE of 65.8% after the initial 2 d operation. This was attributed to the inhibited activities of the AerAOB and AnAOB, whereas an increase in the activities of the DNB was observed at higher C/N ratios. The heterotrophic bacteria competed for O_2 with the AerAOB, and the DNB competed for NO_2^-–N with the AnAOB [28–30]. Thus, the $R_{s:a}$ was increased from 4:8 to 4:10 to increase the DO concentration. After 20 d of operation, the NH_4^+–N concentration in the effluent decreased to 19 mg/L. The ARE and NRE were 90.4% and 84.7%, respectively, and the activities of the AerAOB and AnAOB recovered to 0.123 and 0.179 mgN/(mg MLSS d), respectively.

Subsequently, the C/N ratio was increased to 2.0 in phase XVII. The NH_4^+–N concentration in the effluent increased initially and then decreased to 20 mg/L during the stable operation. The activities of the AerAOB and AnAOB were inhibited and their concentrations decreased to 0.119 and 0.153 mgN/(mg MLSS d), respectively. However, the DNB activity was enhanced, the $DNB_{NO_2^-N}$ was 0.081 mgN/(mg MLSS d), and the $DNB_{NO_3^-N}$ was 0.105 mgN/(mg MLSS d), respectively, which resulted in an NRE greater than 85.8%. Next, the C/N ratio was increased to 3.0 in phase XVIII. The NH_4^+–N concentration in the effluent increased significantly to 85.7 mg/L. The ARE and NRE decreased to 57.2% and 57.5%, respectively, as a result of the strong inhibitions of the AerAOB and AnAOB activities, the values were 0.060 and 0.108 mgN/(mg MLSS d), respectively. It was deduced that the DNB competed with the AnAOB and were dominant in the nitrogen removal process, therefore, the overall nitrogen removal performance was lowest at a C/N ratio of 3.0, which is in agreement with previous reports [31–33].

Finally, the C/N ratio was decreased to 1.0 in phase XIX. After 15 d operation, the activities of the AerAOB and AnAOB recovered to 0.122 and 0.168 mgN/(mg MLSS d), respectively. The DNB activity decreased with an increase

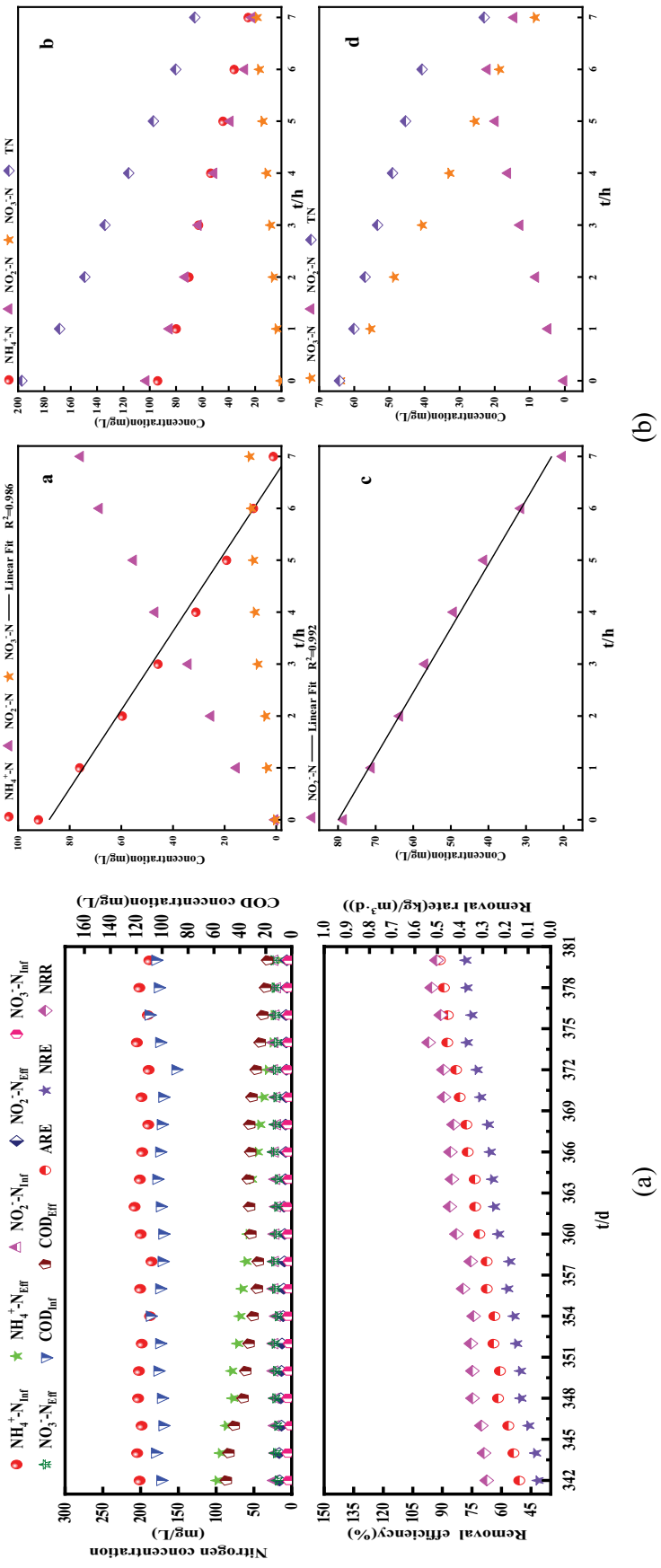

Fig. 4. (a) Performance of the reactor and (b) the activity of the different functional bacteria during the operational phase XIV.

Table 3
Activities of the functional bacteria at different C/N ratios

C/N ratio	AOB mgN/(mg MLSS d)	AnAOB mgN/(mg MLSS d)	$DNB_{NO_2^-N}$ mgN/(mg MLSS d)	$DNB_{NO_3^-N}$ mgN/(mg MLSS d)
0.25	0.126	0.182	0.048	0.079
0.5	0.124	0.180	0.056	0.094
1.0	0.123	0.179	0.064	0.100
2.0	0.119	0.153	0.081	0.105
3.0	0.060	0.108	0.086	0.106
1.0	0.122	0.168	0.064	0.104

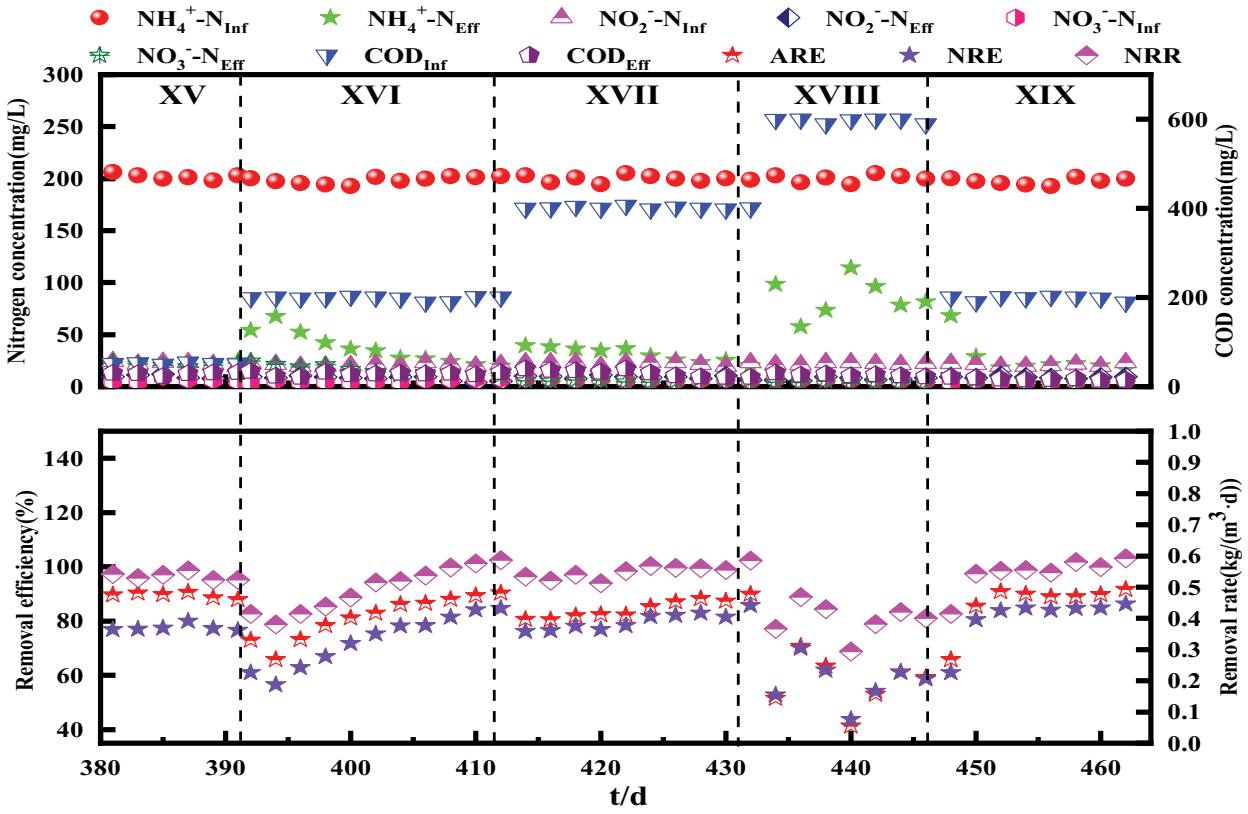

Fig. 5. Performance of the reactor during different operational phases of the SNAD optimization period.

in the C/N ratio, the $DNB_{NO_2^-N}$ was 0.064 mgN/(mg MLSS d) and $DNB_{NO_3^-N}$ was 0.104 mgN/(mg MLSS d), respectively. The optimal synergism of the AerAOB, AnAOB, and DNB was achieved, and the ARE, NRE, and NRR recovered to 91.7%, 86.4%, and 0.59 kg/(m^3 d), respectively.

Based on the results, a model of the nitrogen and COD removal pathways in the SNAD process at a C/N ratio of 1.0 was established (Fig. 6). The model depicts the nitrogen and COD removal pathways and was used to determine the optimal coupling of the nitritation, anammox, and denitrification reactions in the SNAD process. Moreover, compared with heterotrophic denitrification (contribution rate of 35.3%), the model showed that the anammox process was dominant in the nitrogen removal process (contribution rate of 64.7%).

3.3. Membrane fouling

3.3.1. Membrane fouling behaviors

The evolution of the membrane permeability (*L*) and flux (*J*) during different operational phases is shown in Fig. 7. The membrane permeability decreased with increasing filtration time due to membrane fouling. Off-line chemical cleaning was performed when membrane permeability decreased to about 19 L/(m^2 h bar). The membrane fouling rate decreased throughout the operation. The membrane fouling rate was 0.081, 0.079, and 0.077 L/(m^2 h^2 bar) in phase I, phase III, and phase V, respectively, and decreased to 0.065 and 0.052 L/(m^2 h^2 bar) in phase XIII and phase XIX, respectively.

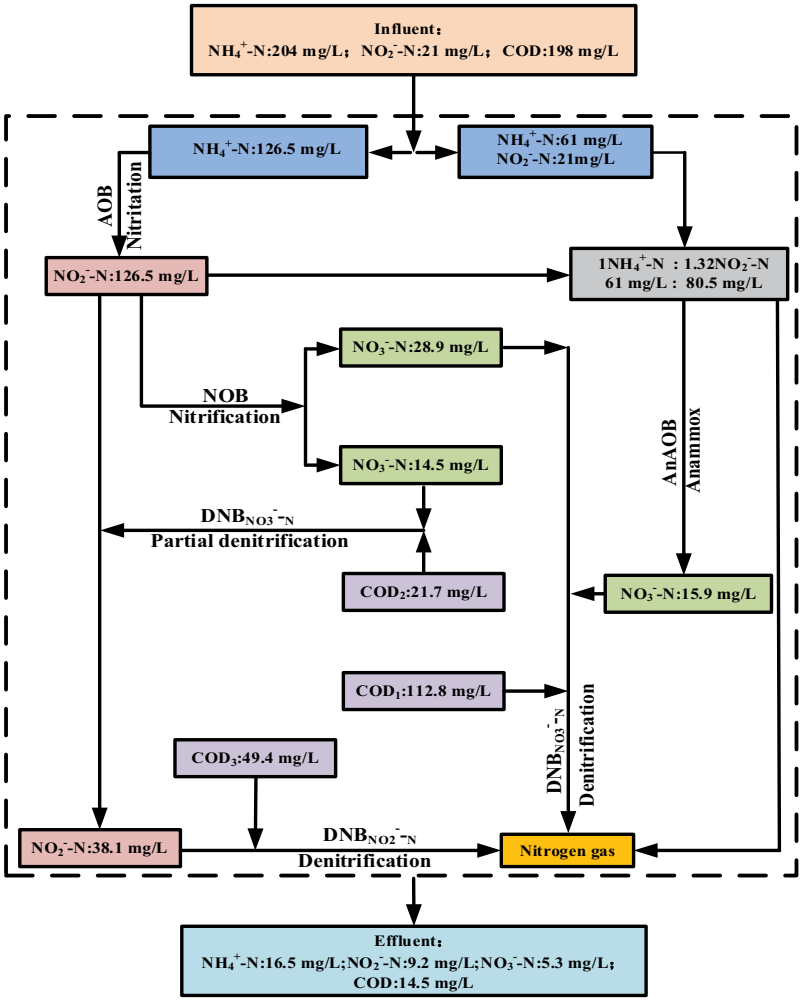

Fig. 6. Model of the nitrogen and COD removal pathway of the SNAD process.

3.3.2. Particle size distribution

The morphological features and particle size distributions of the sludge during different operational phases are shown in Fig. 8. The red sludge flocs had an average particle size of 56.37 and 129.13 μm in phase I and phase III, respectively, resulting in large membrane fouling rates. It has been reported that small-sized sludge particles were prone to be attached to the membrane surface and formed a dense layer that significantly increased the membrane fouling resistance [34]. Dark red micro-granules were formed after the anammox process startup in phase V, and the particle size was mostly below 1.5 mm. This was attributed to the enhanced aggregation of the AnAOB under the high stress of the high nitrogen loading rate [35]. The average particle size increased after the CANON process startup, and the largest proportion was in the range of 1.5–2.0 mm (26.62%). During this phase, the color of the granular sludge changed to light red, which was likely the result of the enrichment of AerAOB on the AnAOB surface [36]. The average particle size increased after the SNAD process startup in phase XIX and the largest proportion (26.67%) was in the range of 2.5–3.0 mm. In this phase, the color of the granular sludge changed to dark red, which was attributed to the enrichment of DNB on the AnAOB surface and the formation of SNAD granules [37]. Overall, the sludge particle size exhibited a trend that was opposite to that of the membrane fouling rate, indicating the importance of the particle size for the mitigation of membrane fouling.

3.3.3. EPS and SMP

The contents and compositions of the EPS and SMP during different operational phases are shown in Fig. 9. The EPS and SMP concentrations exhibited increasing trends, but the rate of increase was higher for the EPS than the SMP, which was the result of organic carbon stress [38]. Specifically, the EPS and SMP concentrations increased from 30.99 mg/g and 23.97 mg/L in phase I to 228.06 mg/g and 50.00 mg/L in phase XIX, respectively. The carbohydrate concentration in the EPS (EPS_p) and the protein concentration in the EPS (EPS_c) increased from 10.33 and 20.66 mg/g to 194.93 and 33.13 mg/g, respectively, and the EPS_p/EPS_c ratio increased from 0.79 to 5.89, indicating that the EPS_p played a predominant role. Similarly, the protein concentration in the SMP (SMP_p) and the carbohydrate concentration in the SMP (SMP_c) increased from 10.35 and 13.62 mg/L to 25.96 and 24.04 mg/L, respectively. It has been reported that

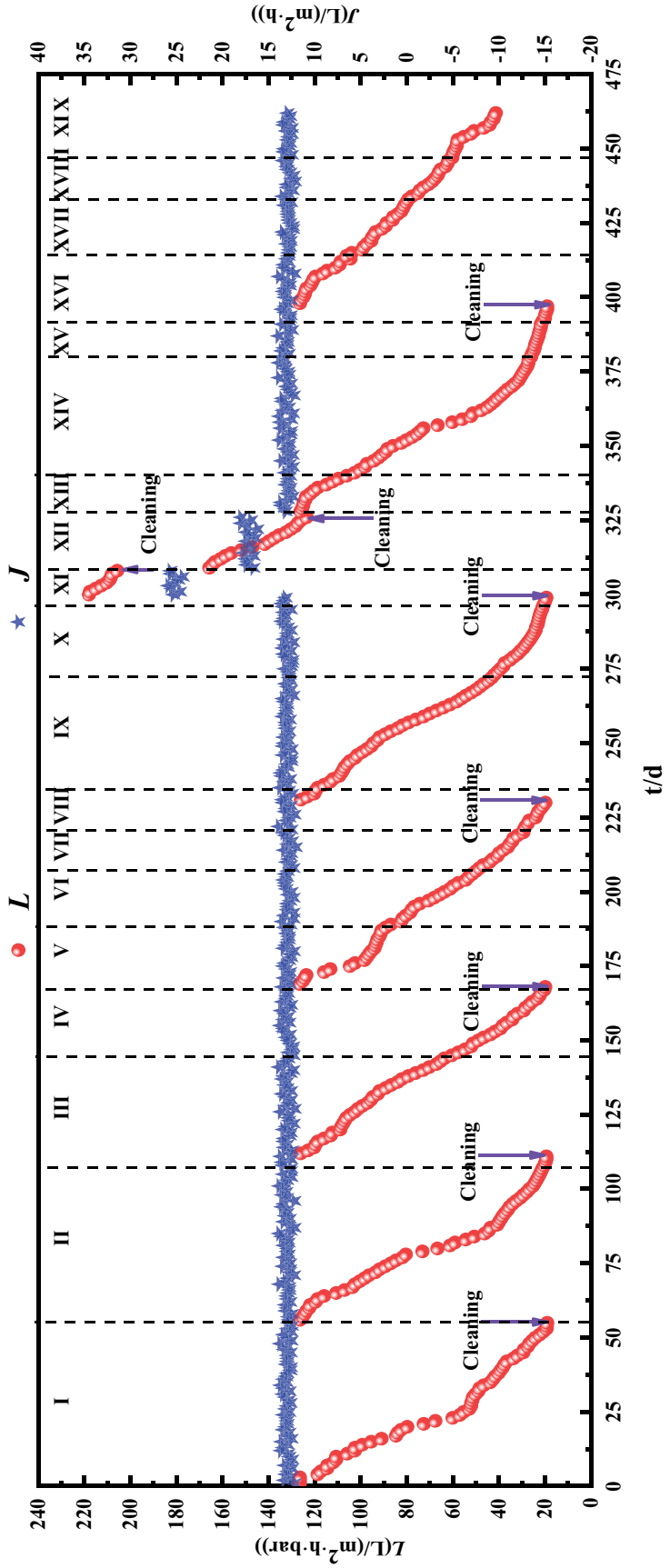

Fig. 7. Evolution of membrane permeability during different operational phases.

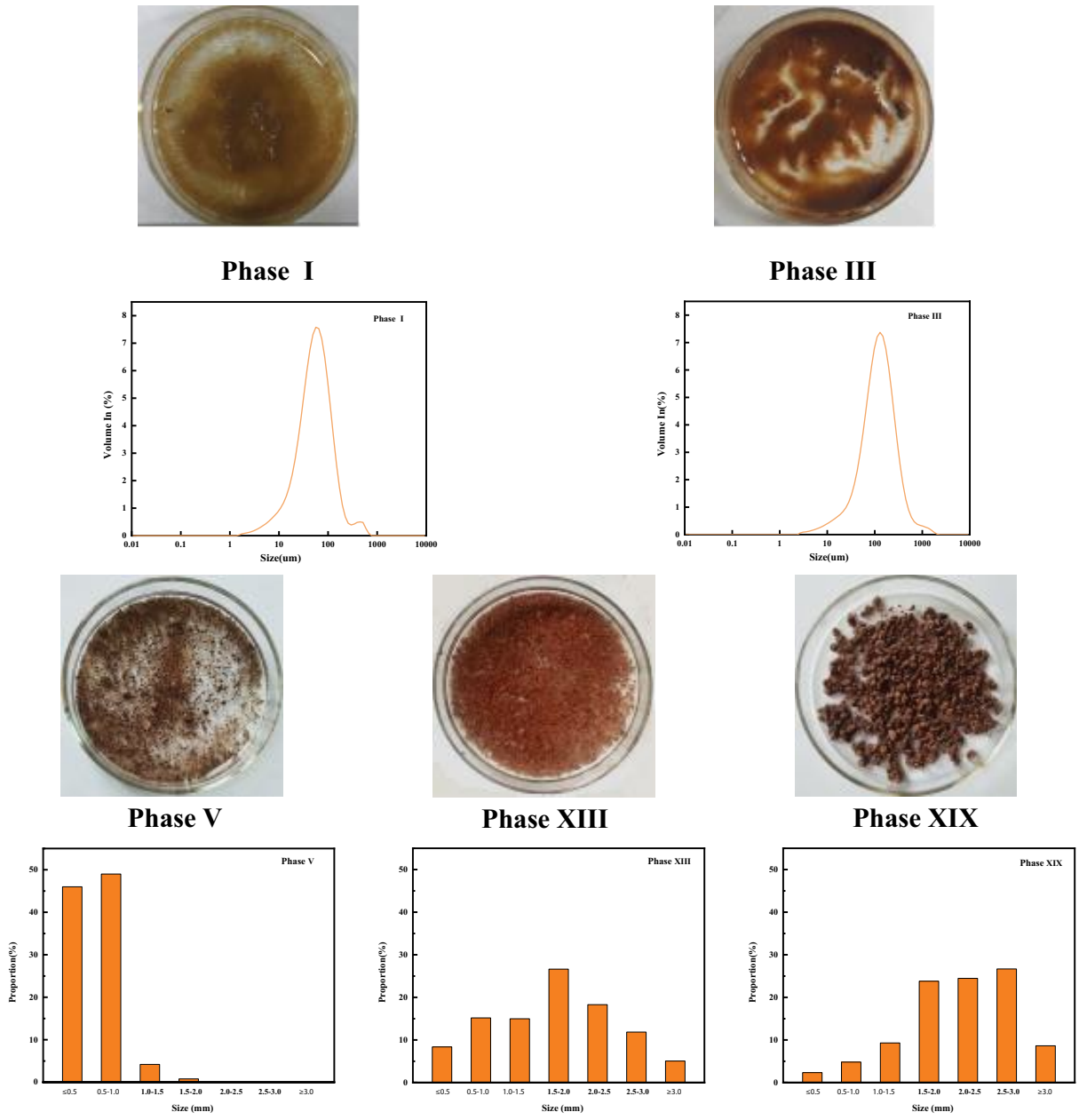

Fig. 8. Morphological features and particle size distributions of the sludge during different operational phases.

sludge aggregation was induced as a result of EPS_p, which decreased the negative charges and increased the hydrophobicity of the sludge surface due to the positive charge of the amino groups [39–41]. Thus, the increase in the EPS content and the EPS_p/EPS_c ratio as a result of the microbial metabolic processes accelerated the sludge granulation and increased the particle size. This mechanism was the main reason for the decrease in the membrane fouling rate and the prolonged operational period.

3.3.4. Sludge settleability

The SVI is an indication of sludge settleability, it is significantly affected by the particle size and indicates the filterability and fouling potential of the sludge mixture. The SVI during different operational phases is shown in Fig. 10. The SVI decreased substantially during the operation and exhibited a trend that was opposite to that of the particle size and EPS content. There was a direct relationship between the sludge particle size and sludge sedimentation, and a theoretical settling formula has been established (Allen's formula) [42]. Deng et al. [43] also found that the SVI had a positive linear relationship with EPS, and granular sludge exhibited good sedimentation performance when the EPS content exceeded 200 mg/g [43]. In this study, the SVI was 95.32 mL/g MLSS for the inoculated sludge, the value decreased to 33.72 mL/g MLSS after the anammox and CANON process startup and finally

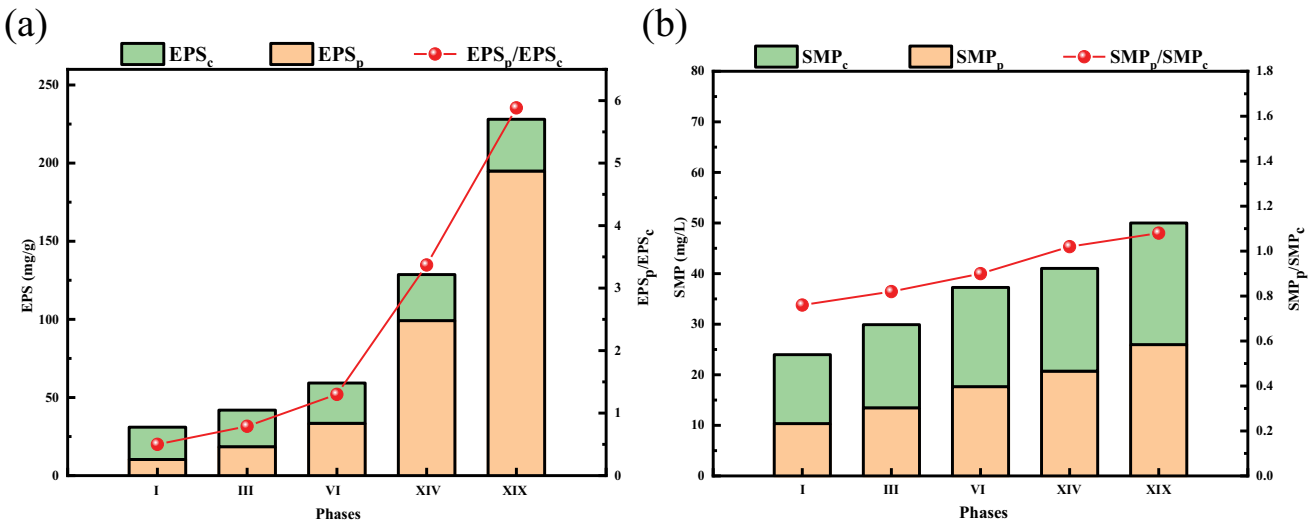

Fig. 9. Carbohydrate and protein contents in the (a) EPS and (b) SMP during different operational phases.

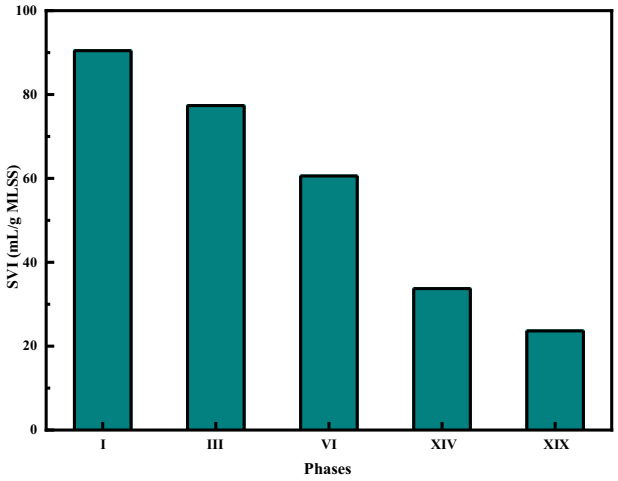

Fig. 10. Sludge volume index (SVI) during different operational phases.

reached 23.63 mL/g MLSS after the SNAD process startup. These results indicate that sludge granulation significantly improved sludge settleability. Compared with floc sludge, granular sludge has better settleability and is not prone to accumulation on the membrane surface and formation of a cake layer, which significantly reduces membrane permeability [44]. Tu et al. [45] also reported similar results and found a good positive correlation between the SVI value and the membrane fouling rate in an immersed MBR process.

3.3.5. FT-IR results of membrane foulants

As shown in Fig. 11, the membrane foulants exhibited similar infrared spectral responses during different operational phases, which suggested similar compositions of the membrane foulants. More specifically, broad absorption peaks were observed at 3,280 and 3,443 cm^{-1}, and these peaks were attributed to the O–H and N–H stretching vibrations, respectively. The peaks at 2,940; 1,654; 1,365 cm^{-1}; and 1,044 cm^{-1} occurred in all infrared spectrum profiles. The peak at 2,940 cm^{-1} was associated with the C–H expansion vibration in the alkane organic matter and carbohydrate molecules, the intensive absorption band at 1,654 cm^{-1} was attributed to the C=O stretching vibration of the protein amide I. The peak at 1,365 cm^{-1} originated from C–H, including the C–OH, CH_3, and CH_2 deformation vibration in the protein structure. The peak at 1,044 cm^{-1} was associated with the C–O–C stretching vibration of carbohydrate-like substances. In addition, absorption peaks were found near the wavelengths of 810 and 579 cm^{-1} in the fingerprint areas. In summary, the membrane foulants mostly consisted of proteins and carbohydrates [46,47].

4. Conclusion

The SNAD process was successfully started up in an MBR by introducing sodium acetate at a C/N ratio of 0.5 following the anammox and CANON processes. The optimal coupling of the nitritation, anammox, and denitrification processes was achieved at a C/N ratio of 1.0, and the ARE, NRE, and CRE were 91.7%, 86.4%, and 85%, respectively. The activity of the functional bacteria indicated the optimal synergism of the AerAOB, AnAOB, and DNB in the SNAD process. The mass balance model of the SNAD process showed that the anammox process played a dominant role in nitrogen removal (contribution rate of 64.7%). The increase in the sludge particle size resulting from sludge granulation was the main reason for the decrease in the membrane fouling rate during the SNAD process. The acceleration of sludge granulation was attributed to the increase in the EPS content and EPS$_p$/EPS$_c$ ratio during the microbial metabolic process. The FT-IR analysis showed that the membrane foulants were mainly composed of proteins and carbohydrates, and few changes were observed during the operation.

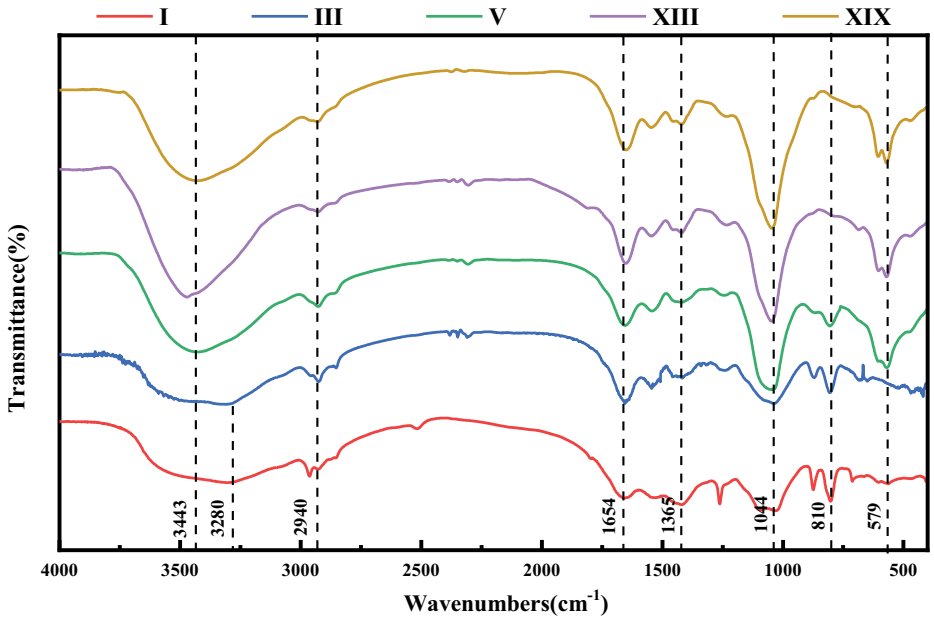

Fig. 11. FT-IR spectra of the membrane foulants during different operational phases

Acknowledgments

This work was financially supported by the Hebei Provincial Natural Science Fund Project (E2016402017), the Project of Young Top Talents Program in Universities and Colleges of Hebei Province (BJ2019029), and the Handan Science and Technology Research and Development plan (1623209044).

References

[1] J. Wu, T. Xu, X.Y. Jiang, G. Yan, L.T. Yu, Model based optimization of partial nitrification by monitoring nitrous oxide (N_2O) emission, J. Environ. Chem. Eng., 3 (2015) 1602–1613.
[2] P. Klangduen, K. Jürg, Study of factors affecting simultaneous nitrification and denitrification (SND), Water Sci. Technol., 39 (1999) 61–68.
[3] J.L. Chen, Y.B. Xu, Y.X. Li, J.S. Liao, J.Y. Ling, J.Y. Li, G.Y. Xie, Effective removal of nitrate by denitrification re-enforced with a two-stage anoxic/oxic (A/O) process from a digested piggery wastewater with a low C/N ratio, J. Environ. Manage., 240 (2019) 19–26.
[4] J.T. Ji, Y.Z. Peng, W.K. Mai, J.Z. He, B. Wang, X.Y. Li, Q. Zhang, Achieving advanced nitrogen removal from low C/N wastewater by combining endogenous partial denitrification with anammox in mainstream treatment, Bioresour. Technol., 270 (2018) 570–579.
[5] Y.H. Liang, D. Li, X.J. Zhang, H.P. Zeng, Z. Yang, S.M. Cui, J. Zhang, Stability and nitrite-oxidizing bacteria community structure in different high-rate CANON reactors, Bioresour. Technol., 175 (2015) 189–194.
[6] J. Pérez, T. Lotti, R. Kleerebezem, C. Picioreanu, M.C.M. Van Loosdrecht, Outcompeting nitrite-oxidizing bacteria in single-stage nitrogen removal in sewage treatment plants: a model-based study, Water Res., 66 (2014) 208–218.
[7] X.L. Li, J. Zhang, X.Y. Zhang, J. Li, F.C. Liu, Y.M. Chen, Start-up and nitrogen removal performance of CANON and SNAD processes in a pilot-scale oxidation ditch reactor, Process Biochem., 84 (2019) 134–142.
[8] X. Yue, G.P. Yu, Y.Q. Lu, Z.H. Liu, Q.H. Li, J.L. Tang, J. Liu, Effect of dissolved oxygen on nitrogen removal and the microbial community of the completely autotrophic nitrogen removal over nitrite process in a submerged aerated biological filter, Bioresour. Technol., 254 (2018) 67–74.
[9] W.G. Wang, Y.Y. Wang, X.D. Wang, Y. Zhang, Y. Yan, Dissolved oxygen microelectrode measurements to develop a more sophisticated intermittent aeration regime control strategy for biofilm-based CANON systems, Chem. Eng. J., 365 (2019) 165–174.
[10] M. Strous, J.J. Heijnen, J.G. Kuenen, M.S.M. Jetten, The sequencing batch reactor as a powerful tool for the study of slowly growing anaerobic ammonium-oxidizing microorganisms, Appl. Microbiol. Biotechnol., 50 (1998) 589–596.
[11] Y. Tao, D.W. Gao, Y. Fu, W.M. Wu, N.Q. Ren, Impact of reactor configuration on anammox process start-up: MBR versus SBR, Bioresour. Technol., 104 (2012) 73–80.
[12] T. Wang, H.M. Zhang, D.W. Gao, F.L. Yang, G.Y. Zhang, Comparison between MBR and SBR on Anammox start-up process from the conventional activated sludge, Bioresour. Technol., 122 (2012) 78–82.
[13] T.L.G. Hendrickx, C. Kampman, G. Zeeman, H. Temmink, Z. Hu, B. Kartal, C.J.N. Buisman, High specific activity for anammox bacteria enriched from activated sludge at 10°C, Bioresour. Technol., 163 (2014) 214–221.
[14] H.H. Chen, S.T. Liu, F.L. Yang, Y. Xue, T. Wang, The development of simultaneous partial nitrification, ANAMMOX and denitrification (SNAD) process in a single reactor for nitrogen removal, Bioresour. Technol., 100 (2009) 1548–1554.
[15] G. Anjali, P.C. Sabumon, Development of simultaneous partial nitrification, anammox and denitrification (SNAD) in a non-aerated SBR, Int. Biodeterior. Biodegrad., 119 (2017) 43–55.
[16] F.Z. Zhang, Y.Z. Peng, L. Miao, Z. Wang, S.Y. Wang, B.K. Li, A novel simultaneous partial nitrification Anammox and denitrification (SNAD) with intermittent aeration for cost-effective nitrogen removal from mature landfill leachate, Chem. Eng. J., 313 (2017) 619–628.
[17] G. Wang, X.C. Xu, Z. Gong, F. Gao, F.L. Yang, H.M. Zhang, Study of simultaneous partial nitrification, ANAMMOX and denitrification (SNAD) process in an intermittent aeration membrane bioreactor, Process Biochem., 51 (2016) 632–641.

[18] C.Q. Zhao, G. Wang, X.C. Xu, Y.S. Yang, F.L. Yang, Long-term operation of oxygen-limiting membrane bioreactor (MBR) for the development of simultaneous partial nitrification, anammox and denitrification (SNAD) process, Environ. Technol., 39 (2018) 2193–2202.
[19] APHA-American Public Health Association, AWWA-American Water Works Association, WEF-Water Environment Federation, Standard Methods for the Examination of Water and Wastewater, 21st ed., Washington DC, USA, 2005.
[20] A. Laguna, A. Ouattara, R.O. Gonzalez, O. Baron, G. Famá, R.E. Mamouni, S. Guiot, O. Monroy, H. Macarie, A simple and low cost technique for determining the granulometry of upflow anaerobic sludge blanket reactor sludge, Water Sci. Technol., 40 (1999) 1–8.
[21] C.J. Tang, P. Zheng, Q. Mahmood, J.W. Chen, Start-up and inhibition analysis of the Anammox process seeded with anaerobic granular sludge, J. Ind. Microbiol. Biotechnol., 36 (2009) 1093–1100.
[22] Z.M. Zheng, J. Li, J. Ma, J. Du, W. Bian, Y. Li, Y.Z. Zhang, B.H. Zhao, Nitrogen removal via simultaneous partial nitrification, anammox and denitrification (SNAD) process under high DO condition, Biodegradation, 27 (2016) 195–208.
[23] F. Fang, M.M. Yang, H. Wang, P. Yan, Y.P. Chen, J.S. Guo, Effect of high salinity in wastewater on surface properties of anammox granular sludge, Chemosphere, 210 (2018) 366–375.
[24] J. Wu, H.M. Zhou, H.Z. Li, P.C. Zhang, J. Jiang, Impacts of hydrodynamic shear force on nucleation of flocculent sludge in anaerobic reactor, Water Res., 43 (2009) 3029–3036.
[25] D. Seuntjens, J.M. Carvajal-Arroyo, M. Ruopp, P. Bunse, C.P. De Mulder, S. Lochmatter, S. Agrawal, N. Boon, S. Lackner, S.E. Vlaeminck, High-resolution mapping and modeling of anammox recovery from recurrent oxygen exposure, Water Res., 144 (2018) 522–531.
[26] L.H. Ye, D. Li, J. Zhang, H.P. Zeng, Resuscitation of starved anaerobic ammonium oxidation sludge system: impacts of repeated short-term starvation, Bioresour. Technol., 263 (2018) 458–466.
[27] J.R. Vázquez-Padín, M.J. Pozo, M. Jarpa, M. Figueroa, A. Franco, A. Mosquera-Corral, J.L. Campos, R. Méndeza, Treatment of anaerobic sludge digester effluents by the CANON process in an air pulsing SBR, J. Hazard. Mater., 166 (2009) 336–341.
[28] E.I.P. Volcke, C. Picioreanu, B. De Baets, M.C.M. van Loosdrecht, Effect of granule size on autotrophic nitrogen removal in a granular sludge reactor, Environ. Technol., 31 (2010) 1271–1280.
[29] M.K.H. Winkler, J.J. Yang, R. Kleerebezem, E. Plaza, J. Trela, B. Hultman, M.C.M. van Loosdrechta, Nitrate reduction by organotrophic Anammox bacteria in a nitritation/anammox granular sludge and a moving bed biofilm reactor, Bioresour. Technol., 114 (2012) 217–223.
[30] J.R. Vázquez-Padín, I. Fernández, N. Morales, J.L. Campos, A. Mosquera-Corral, R. Méndez, Autotrophic nitrogen removal at low temperature, Water Sci. Technol., 63 (2011) 1282–1288.
[31] Y.Y. Miao, Y.Z. Peng, L. Zhang, B.K. Li, X.Y. Li, L. Wu, S.M. Wang, Partial nitrification-anammox (PNA) treating sewage with intermittent aeration mode: effect of influent C/N ratios, Chem. Eng. J., 334 (2018) 664–672.
[32] C.J. Tang, P. Zheng, C.H. Wang, Q. Mahmood, Suppression of anaerobic ammonium oxidizers under high organic content in high-rate Anammox UASB reactor, Bioresour. Technol., 101 (2010) 1762–1768.
[33] S.Q. Ni, J.Y. Ni, D.L. Hu, S. Sung, Effect of organic matter on the performance of granular anammox process, Bioresour. Technol., 110 (2012) 701–705.
[34] Y. Satyawali, M. Balakrishnan, Effect of PAC addition on sludge properties in a MBR treating high strength wastewater, Water Res., 43 (2009) 1577–1588.
[35] U. Manonmani, K. Joseph, Granulation of anammox microorganisms for autotrophic nitrogen removal from wastewater, Environ. Chem. Lett., 16 (2018) 881–901.
[36] F.Y. Qian, J.F. Wang, Y.L. Shen, Y. Wang, S.Y. Wang, X. Chen, Achieving high performance completely autotrophic nitrogen removal in a continuous granular sludge reactor, Biochem. Eng. J., 118 (2017) 97–104.
[37] B.L. Li, Y. Wang, J.T. Li, L. Yang, X. Li, Z. Zhou, Y. Li, X.G. Chen, L. Wu, The symbiosis of anaerobic ammonium oxidation bacteria and heterotrophic denitrification bacteria in a size-fractioned single-stage partial nitrification/anammox reactor, Biochem. Eng. J., 151 (2019) 1–9.
[38] X.L. Ho, S.T. Liu, Z.T. Zhang, Role of extracellular polymeric substance in determining the high aggregation ability of anammox sludge, Water Res.,75 (2015) 51–62.
[39] S.Q. Ni, N. Sun, H.L. Yang, J. Zhang, H.H. Ngo, Distribution of extracellular polymeric substances in anammox granules and their important roles during anammox granulation, Biochem. Eng. J., 101 (2015) 126–133.
[40] S.Q. Ni, A. Fessehaie, P.H. Lee, B.Y. Gao, X. Xu, S. Sung, Interaction of anammox bacteria and inactive methanogenic granules under high nitrogen selective pressure, Bioresour. Technol., 101 (2010) 6910–6915.
[41] L.L. Zhang, X.X. Feng, N.W. Zhu, J.M. Chen, Role of extracellular protein in the for mation and stability of aerobic granules, Enzyme Microb. Technol., 41 (2007) 551–557.
[42] F.A. Tassew, W.H. Bergland, C. Dinamarca, R. Bakke, Settling velocity and size distribution measurement of anaerobic granular sludge using microscopic image analysis, J. Microbiol. Methods, 159 (2019) 81–90.
[43] S. Deng, L.X. Wang, H.J. Su, Role and influence of extracellular polymeric substances on the preparation of aerobic granular sludge, J. Environ. Manage., 173 (2016) 49–54.
[44] K.M. Wang, A. Soares, B. Jefferson, E.J. McAdam, Comparable membrane permeability can be achieved in granular and flocculent anaerobic membrane bioreactor for sewage treatment through better sludge blanket control, J. Water Process Eng., 28 (2019) 181–189.
[45] X. Tu, S. Zhang, L.R. Xu, M.C. Zhang, J.R. Zhu, Performance and fouling characteristics in a membrane sequence batch reactor (MSBR) system coupled with aerobic granular sludge, Desalination, 261 (2010) 191–196.
[46] J.P. Croué, M.F. Benedetti, D. Violleau, J.A. Leenheer, Characterization and copper binding of humic and nonhumic organic matter isolated from South Platte River: evidence for the presence of nitrogenous binding site, Environ. Sci. Technol., 37 (2003) 328–336.
[47] M. Kumar, S.S. Adham, W.R. Pearce, Investigation of seawater reverse osmosis fouling and its relationship to pretreatment type, Environ. Sci. Technol., 40 (2006) 2037–2044.